SPE
Society of Petroleum Engineers of AIME

SPE 12241

Simulation of Miscible Displacement Using Mixed Methods and a Modified Method of Characteristics

by R.E. Ewing, *U. of Wyoming;* T.F. Russell, *Marathon Oil Co.;* and M.F. Wheeler, *Rice U.*

Members SPE-AIME

This paper was presented at the Reservoir Simulation Symposium held in San Francisco, CA, November 15–18, 1983. The material is subject to correction by the author. Permission to copy is restricted to an abstract of not more than 300 words. Write SPE, 6200 North Central Expressway, Drawer 64706, Dallas, Texas 75206 USA. Telex 730989 SPEDAL.

ABSTRACT

Numerical dispersion and grid orientation problems with adverse mobility ratios are two of the major difficulties in the numerical simulation of enhanced recovery processes. An efficient method for modeling convection-dominated flows which greatly reduces numerical dispersion and grid orientation problems is presented and applied to miscible displacement in a porous medium. The base method utilizes characteristic flow directions to model convection and finite elements to treat the diffusion and dispersion. The characteristic approach also minimizes certain overshoot difficulties which accompany many finite element methods for problems with sharp fluid interfaces. The truncation error caused by the characteristic time-stepping technique is small, so large stable time-steps can be taken as in fully-implicit methods without the corresponding loss in accuracy. A finite difference analogue can also be formulated.

Since the computed fluid velocities help to determine the time-stepping procedure in the characteristic-based method and since accurate velocities are crucial in the method's ability to conserve mass, very accurate Darcy velocities are necessary. A mixed finite element method solves for the pressure and the Darcy velocity simultaneously, as a system of first order partial differential equations. By solving for $u = -(k/\mu)\nabla p$ as one term, we minimize the difficulties occurring in standard methods caused by differentiation or differencing of p and multiplying by rough coefficients k/μ.

Using a combination of characteristic-based time-stepping procedures and mixed methods for accurate velocities, a variety of problems with variable (or random) permeabilities, adverse mobility ratios, and tensor dispersion models are examined. A study of viscous fingering is presented. Computational results on a variety of two-dimensional problems show minimal grid-orientation effects, reduced numerical dispersion, minimal overshoot at the front, and very low mass balance errors.

References and illustrations at end of paper.

INTRODUCTION

We shall discuss accurate time-stepping procedures for coupled systems of partial differential equations arising in reservoir simulation. We shall formulate our methods in the context of miscible displacement problems in porous media. Similar techniques are applicable for a wide variety of secondary and tertiary enhanced recovery procedures involving transport-dominated processes. Although we shall define method-of-characteristics-based finite difference time-stepping procedures in a coupled setting with finite element spatial methods, similar techniques can be formulated for finite difference spatial methods.

In convection-diffusion equations, such as the concentration equation for miscible displacement problems, when convection dominates diffusion, standard finite difference or finite element procedures suffer from numerical dispersion, overshoot, and grid orientation difficulties. References 1 and 2 contain extensive bibliographies of work in this area. A different procedure, which concentrates on treating the convective terms efficiently and accurately, is presented. Our procedure, a modification of the method of characteristics which is so useful for hyperbolic equations, takes time steps in the direction of flow, along the characteristics of the velocity field of the total fluid. It then accounts for physical diffusion or dispersion in a more standard fashion. This amounts to a type of physical splitting of the spatial operator.

The key to the ease of implementation of this technique is that we look backward in time, along an approximate flow path, instead of forward in time as in many methods of characteristics or moving mesh techniques. Thus the points at which the unknowns are determined need not change in time (though they may if desired) and stay in a regular grid pattern; no complex data structure is required to keep track of moving grid points. This makes implementation of these techniques significantly easier, in two and three space dimensions, than moving mesh methods. We extrapolate the velocity field in time from previous time levels to obtain an approximation to the velocity field at the advanced level along which to proceed in time. Since the

time-stepping direction is along a characteristic where the unknowns are changing slowly, larger time steps can be taken without introducing serious time-truncation errors.

MODEL PROBLEM

We shall consider a model problem describing the displacement of one incompressible fluid by another, totally miscible with the first, in a horizontal porous reservoir $\Omega \subset \mathbf{R}^2$ over a time period $J = [0, T]$. If c is the concentration of the invading fluid and p and $\underset{\sim}{u}$ are the pressure and Darcy velocity of the total fluid, then a model system of coupled quasilinear partial differential equations relating c, p, and $\underset{\sim}{u}$ is given by[3]

$$(1) \quad -\nabla \cdot \left[\frac{k}{\mu} \nabla p\right] \equiv \nabla \cdot \underset{\sim}{u} = q \qquad , \underset{\sim}{x}\in\Omega,\ t\in J,$$

$$(2) \quad \phi \frac{\partial c}{\partial t} - \nabla \cdot \left[\underset{\approx}{D} \nabla c - \underset{\sim}{u}\, c\right] = q\,\tilde{c} \qquad , \underset{\sim}{x}\in\Omega,\ t\in J.$$

The symbols in (1) and (2) are defined in the nomenclature section. The diffusion-dispersion tensor $\underset{\approx}{D}(\underset{\sim}{x}, \underset{\sim}{u})$ takes the form[4]

$$(3) \quad \underset{\approx}{D} = \begin{pmatrix} D_{11} & D_{12} \\ D_{21} & D_{22} \end{pmatrix} = \phi(\underset{\sim}{x})\, d_m\, I + \frac{d_\ell}{|\underset{\sim}{u}|} \begin{pmatrix} u_1^2 & u_1u_2 \\ u_1u_2 & u_1^2 \end{pmatrix} + \frac{d_t}{|\underset{\sim}{u}|} \begin{pmatrix} u_2^2 & -u_1u_2 \\ -u_1u_2 & u_1^2 \end{pmatrix}$$

where d_m, a molecular diffusion coefficient, and d_ℓ and d_t, the magnitudes of longitudinal and transverse dispersion, are constants determined empirically. Laboratory experiments have found that the longitudinal dispersivity d_ℓ is typically considerably greater than the transverse dispersivity d_t, and that the molecular diffusion coefficient is very small by comparison. The viscosity μ is determined by the following mixing rule:

$$(4) \quad \mu(c) = \mu(o)\left((c^{1/4} - 1)\, M + 1\right)^{-4}.$$

Therefore the viscosity changes very rapidly, with the concentration, in the neighborhood of the moving fluid interface and is fairly constant away from the front. In addition to (1)-(4), we prescribe an initial concentration of the invading fluid,

$$(5) \quad c(\underset{\sim}{x}, o) = c_o(\underset{\sim}{x}) \qquad , \underset{\sim}{x}\in\Omega,$$

and no-flow boundary conditions

$$(6) \quad \underset{\sim}{u} \cdot \underset{\sim}{\nu} = 0 \qquad , \underset{\sim}{x}\in\partial\Omega,\ t\in J,$$

$$(7) \quad \sum_{i,j=1}^{2} D_{ij}(\underset{\sim}{x}, \underset{\sim}{u}) \frac{\partial c}{\partial x_j} \nu_i = 0 \qquad , \underset{\sim}{x}\in\partial\Omega,\ t\in J.$$

Expanding the $\nabla \cdot \underset{\sim}{u}c$ term in (2) using the chain rule for differentiation and then using (1) to replace $\underset{\sim}{u}$ in the result, we obtain the following non-divergence form of (1)-(2):

$$(8) \quad -\nabla \cdot \left[\frac{k}{\mu} \nabla p\right] \equiv \nabla \cdot \underset{\sim}{u} = q \qquad , \underset{\sim}{x}\in\Omega,\ t\in J,$$

$$(9) \quad \phi \frac{\partial c}{\partial t} - \nabla \cdot (\underset{\approx}{D} \nabla c) + \underset{\sim}{u} \cdot \nabla c = (\tilde{c} - c)q \qquad , \underset{\sim}{x}\in\Omega,\ t\in J.$$

Note that (9) is the same as (2) away from the wells. The equation (9) is a convection-diffusion equation with the relative importance of diffusion or dispersion indicated by the size of the coefficients d_m, d_ℓ, and d_t. If these coefficients are very small, the effective Peclet number of the problem is large and sharp traveling interfaces between the injected and resident fluids diffuse slowly as they move through the reservoir. Upstream-weighted finite difference methods for this problem tend to introduce an artificial numerical dispersion which is not rotationally invariant. This dispersion tends to smear the sharp traveling fronts unphysically while the directional dependence causes grid-orientation effects to appear in the solution. The time-stepping method presented here stabilizes the problem (avoids significant overshoot and oscillations), without the introduction of an artificial, directionally dependent numerical dispersion, by incorporating the transport term in the time-stepping operator.

TIME DISCRETIZATION USING CHARACTERISTICS

If we neglect the diffusion term, the unit vector in the characteristic direction is

$$(10) \quad \tau(\underset{\sim}{x}, t) = \left(\frac{\underset{\sim}{u}(\underset{\sim}{x}, t)}{\sqrt{\phi(\underset{\sim}{x})^2 + |\underset{\sim}{u}(\underset{\sim}{x}, t)|^2}}, \frac{\phi(\underset{\sim}{x})}{\sqrt{\phi^2 + |\underset{\sim}{u}(\underset{\sim}{x}, t)|^2}}\right)$$

in the $(\underset{\sim}{x}, t)$-coordinates. This vector is illustrated in Figure 1. The directional derivative in the τ-direction is therefore

$$(11) \quad \frac{\partial}{\partial \tau} = \frac{1}{\sqrt{\phi(\underset{\sim}{x})^2 + |\underset{\sim}{u}(\underset{\sim}{x}, t)|^2}} \left(\phi(\underset{\sim}{x}) \frac{\partial}{\partial t} + \underset{\sim}{u}(\underset{\sim}{x}, t) \cdot \nabla\right).$$

We then use (11) to replace the first and third terms in (9) and obtain the system

$$(12) \quad -\nabla \cdot \left(\frac{k}{\mu} \nabla p\right) \equiv \nabla \cdot u = q \qquad , \underset{\sim}{x}\in\Omega,\ t\in J,$$

$$(13) \quad \sqrt{\phi(\underset{\sim}{x})^2 + |\underset{\sim}{u}(\underset{\sim}{x}, t)|^2} \frac{\partial c}{\partial \tau} - \nabla \cdot (\underset{\approx}{D} \nabla c) = (\tilde{c} - c)q \qquad , \underset{\sim}{x}\in\Omega,\ t\in J.$$

In the $(\underset{\sim}{x}, \tau)$-coordinate system, (13) has the form of a diffusion equation with no convection term. We then apply a finite element spatial discretization procedure coupled with a backward differencing in the "time" variable τ to this new system of partial differential equations.

Let Δt denote the time step and $t^n = n\Delta t$ with $T = N\Delta t$. Then the backward difference approximation of the characteristic derivative $(\partial c/\partial \tau)(\underset{\sim}{x}, t^{n+1})$ along the characteristic is given by

$$(14)\quad \frac{\partial c}{\partial \tau}(\underset{\sim}{x}, t^{n+1}) \approx \frac{c(\underset{\sim}{x}, t^{n+1}) - c\left(\underset{\sim}{x} - \frac{\underset{\sim}{\underset{\sim}{u^*}}(x)}{\phi(x)}\Delta t, t^n\right)}{\sqrt{\phi(x)^2 + |\underset{\sim}{\underset{\sim}{u}}(x, t)|^2}\,\Delta t}.$$

In (14), $\underset{\sim}{u}^*$ is an approximate average velocity of a fluid particle reaching $\underset{\sim}{x}$ at time t^{n+1}; the procedure for calculating this average is described below. Using (14) in (13) we obtain

$$(15)\quad \sqrt{\phi(x)^2 + |\underset{\sim}{\underset{\sim}{u}}(x, t)|^2}\,\frac{\partial c}{\partial \tau}(x, t^{n+1}) \approx \frac{c(\underset{\sim}{x}, t^{n+1}) - c\left(\underset{\sim}{x} - \frac{\underset{\sim}{\underset{\sim}{u^*}}(x)}{\phi(x)}\Delta t, t^n\right)}{\Delta t}$$

as our new accumulation term in (13). Clearly, for this difference quotient to be useful, we must be able to determine $\underset{\sim}{u}^*(\underset{\sim}{x})$. The forthcoming description refers to $\underset{\sim}{u}$; of course, the actual computation will use a numerical velocity field $\underset{\sim}{U}$ to be calculated by procedures described in later sections. We shall extrapolate $\underset{\sim}{u}$ from the last two time levels to obtain, as an approximation to $\underset{\sim}{u}(\underset{\sim}{x}, t^{n+1})$,

$$(16)\quad E\underset{\sim}{\underset{\sim}{u}}(\underset{\sim}{x}, t^{n+1}) = 2\underset{\sim}{\underset{\sim}{u}}(\underset{\sim}{x}, t^n) - \underset{\sim}{\underset{\sim}{u}}(\underset{\sim}{x}, t^{n-1}),\ n \geq 1,$$

$$(17)\quad E\underset{\sim}{\underset{\sim}{u}}(\underset{\sim}{x}, t^1) = \underset{\sim}{\underset{\sim}{u}}(\underset{\sim}{x}, t^0).$$

If we are not using a uniform time step in our method, an appropriate modification must be made in (16) to obtain the correct linear extrapolation from the two previous time steps.

Segmenting Description

To compute $\underset{\sim}{u}^*$ accurately, particularly near wells where $\underset{\sim}{u}$ varies rapidly in space, we trace along the characteristic using micro-time steps. First we interpolate linearly in time between $\underset{\sim}{u}(\underset{\sim}{x}, t^n)$ and $E\underset{\sim}{u}(\underset{\sim}{x}, t^{n+1})$ to obtain values for $\underset{\sim}{u}$ at intermediate times. Next, where $\underset{\sim}{u}$ is discontinuous (as shown in a later section, this occurs at element boundaries if $\underset{\sim}{u}$ is approximated by a mixed finite element method) in space, we average the values on either side of the jump if we are very close to the jump (e.g., within 1% of the distance between jumps).

Working backward in time, we begin at t^{n+1} and choose time steps $\Delta t_1, \Delta t_2, \ldots, \Delta t_m$ that sum to Δt. The method of choosing these is described below. Let $t_k = t^{n+1} - \Delta t_1 - \ldots - \Delta t_k$ be the kth intermediate step, with $t_0 = t^{n+1}$, $t_m = t^n$. To evaluate $\underset{\sim}{u}^*(\underset{\sim}{x})$, start the iteration with $\underset{\sim}{x}_0 = \underset{\sim}{x}$. Given $\underset{\sim}{x}_{k-1}$, we find $\underset{\sim}{x}_k$ by a predictor-corrector procedure:

$$\underset{\sim}{x}'_k = \underset{\sim}{x}_{k-1} - \frac{\underset{\sim}{u}(\underset{\sim}{x}_{k-1}, t_{k-1})}{\phi(\underset{\sim}{x}_{k-1})}\Delta t_k \qquad \text{(predictor)},$$

$$\underset{\sim}{x}_k = \underset{\sim}{x}_{k-1} - \frac{1}{2}\left(\frac{\underset{\sim}{u}(\underset{\sim}{x}_{k-1}, t_{k-1})}{\phi(\underset{\sim}{x}_{k-1})} + \frac{\underset{\sim}{u}(\underset{\sim}{x}'_k, t_k)}{\phi(\underset{\sim}{x}')}\right)\Delta t_k \qquad \text{(corrector)}.$$

If $\underset{\sim}{x}_k$ reaches across $\partial\Omega$, use the no-flow boundary condition as a reflection to bring it back. The average interstitial velocity in the corrector attempts to approximate a chord along the characteristic curve. Finally, set

$$(18)\quad \bar{\underset{\sim}{x}} = \underset{\sim}{x}_m = \underset{\sim}{x} - \frac{\underset{\sim}{\underset{\sim}{u^*}}(x)}{\phi(x)}\Delta t.$$

This defines $\underset{\sim}{u}^*(\underset{\sim}{x})$ and identifies the point $\bar{\underset{\sim}{x}}$ at time t^n that flows to $\underset{\sim}{x}$ at t^{n+1} according to the approximate average velocity $\underset{\sim}{u}^*(\underset{\sim}{x})$.

It remains to show how Δt_k is chosen. This is done via a crude error estimator that assumes that the velocity field behaves like the inverse of the distance to the nearest well. This is a poor approximation far from the wells, but that is not important because $m = 1$ at such locations anyway. With some elementary calculus, one can show that the average corrector velocity will differ from the true average velocity by about 1% if the path from $\underset{\sim}{x}_{k-1}$ to $\underset{\sim}{x}'_k$ multiplies the distance from a producer by 5/3 or from an injector by 2/3. We use the predictor equation to make Δt_k satisfy these constraints; if $t_{k-1} - t^n$ is smaller, we set Δt_k to that value to finish the overall time step Δt. By similar ideas, it is possible to tell whether a characteristic will reach back to an injector; if so, simply place $\bar{\underset{\sim}{x}}$ at the injector and stop the iteration.

The time-stepping procedure defined by (14) or (15) will require the evaluation of c at $\bar{\underset{\sim}{x}}$ at time level t^n. Since this point will, in general, not be a spatial grid point, we must either evaluate the function c produced by the finite element spatial procedure at this point or, if finite difference methods have been used, interpolate the finite difference approximation given only at grid points to obtain $c(\bar{\underset{\sim}{x}}, t^n)$. As will be discussed in more detail in later sections, this interpolation can give rise to small mass balance errors and must be treated carefully.

SPATIAL DISCRETIZATION

Although the use of finite element spatial discretization would allow a general finite element mesh with triangles, curvilinear polygons, or other grids to more easily approximate curved boundaries of the reservoir or flow and potential lines, in this study, we shall restrict ourselves to the use of tensor product spaces on rectangles. For illustrative purposes, let $\Omega = [a_x, b_x] \times [a_y, b_y]$ and take

$$(19)\quad \Delta_x = \{a_x = x_0 < x_1 < \ldots < x_{N_x} = b_x\}\ ,$$

$$(20)\quad \Delta_y = \{a_y = y_0 < y_1 < \ldots < y_{N_y} = b_y\}\ ,$$

as subdivisions in x and y, respectively. Let $v_i(x)$, $0 \le i \le N_x$, and $w_j(y)$, $0 \le j \le N_y$, denote the one-dimensional piecewise linear basis functions in each direction which are equal to one at the indexed node and zero at all other nodes. Then the spaces of trial functions and test functions in the Galerkin procedure will consist of all linear combinations of the form

$$(21)\quad C^n(x, y) = \sum_{i=0}^{N_x}\sum_{j=0}^{N_y} \beta_{ij}^n\, v_i(x)\, w_j(y)\ ,$$

where, as before, the superscript n denotes that the approximation is taken at the time level t^n. Again we emphasize that the spatial grids, and hence the finite element spaces, need not change with n, but the coefficients β_{ij}^n do change in time. The functions described by (21) are continuous, and are piecewise linear along any line parallel to either the x-axis or the y-axis.

For notational purposes, using the partition Δ_x^c for the concentration equation (superscript c indicating concentration), we define the space

$$(22)\quad M_j^m(\Delta_x^c) \equiv \{\psi \varepsilon C^j([a_x, b_x]) : \psi|_{[x_{i-1}, x_i]} \varepsilon P_m\ ,\ i=1, \ldots, N_x\}\ .$$

Using this notation the space of continuous bilinear piecewise polynomials described above can be written as $M_0^1(\Delta_x^c) \otimes M_0^1(\Delta_y^c)$. We shall use this space for both trail and test spaces for the concentration equation and shall thus denote it by M_c.

The time-stepping method discussed here was first introduced by one of the authors into the SPE literature in Ref. 5. In that paper, a less accurate method of tracing characteristics was used. We will compare some of the results of that paper with those obtained here. Thus, for completeness, we shall first recall the spatial discretization used for the pressure equation in Ref. 5. Since the logarithmic singularities are so important to the description of the pressure behavior, the technique of adding special functions around the wells, described in Ref. 5, was incorporated in the piecewise biquadratic polynomials used as a pressure space in Ref. 5. Biquadratic polynomials are presented in detail in Ref. 2 and will not be further described here. The trial and test space used in Ref. 5 for the pressure equation (1) is denoted by M_p. We shall define different trial and test spaces used to approximate both the pressure and Darcy velocity simultaneously via a mixed finite element method in the next section.

Again, we emphasize that a finite difference spatial discretization can be easily used in conjunction with the modified method of characteristics time-stepping scheme. For details of how these techniques apply to convection-diffusion equations in a more general setting, see Ref. 7. In order to handle the dispersion tensor, a finite difference method must be a nine-point scheme. The computational effort of a nine-point scheme is similar to that for the finite element methods presented here.

Combining the modified method of characteristics with standard finite element methods as discussed in Ref. 5 yields the following fully-discrete finite element procedure: Find C^n, $n = 1, \ldots, N \in M_c$ satisfying

$$(23)\quad \iint_\Omega \Big[\phi \frac{C^{n+1}(\underset{\sim}{x}) - C^n(\bar{\underset{\sim}{x}})}{\Delta t}\theta + D_{11}(\underset{\sim}{x}, \underset{\sim}{U}^*)\frac{\partial C^{n+1}}{\partial x}\frac{\partial \theta}{\partial x} + D_{12}(\underset{\sim}{x}, \underset{\sim}{U}^*)\Big\{\frac{\partial C^{n+1}}{\partial x}\frac{\partial \theta}{\partial y} + \frac{\partial C^{n+1}}{\partial y}\frac{\partial \theta}{\partial x}\Big\} + D_{22}(\underset{\sim}{x}, \underset{\sim}{U}^*)\frac{\partial C^{n+1}}{\partial y}\frac{\partial \theta}{\partial y}\Big]\, d\underset{\sim}{x} = \iint_\Omega (\tilde{C}^{n+1} - C^{n+1})\, q^{n+1}\, \theta\, d\underset{\sim}{x}\ ,\quad \theta \varepsilon M_c,$$

where $\underset{\sim}{U}^*$ denotes the approximate average Darcy velocities defined from the computed pressures P^n and P^{n-1} using

$$(24)\quad \underset{\sim}{U}^k(\underset{\sim}{x}) = -\frac{\underset{\sim}{k}(\underset{\sim}{x})}{\mu(C^k)}\nabla P^k\ ,\quad k=n,\ n-1,$$

and the extrapolation from (16). The pressures are approximated from M_p, in turn, at the new time level t^{n+1} by solving

$$(25)\quad \iint_\Omega \frac{\underset{\sim}{k}}{\mu}\nabla P^{n+1}\cdot\nabla \chi\, d\underset{\sim}{x} = \iint_\Omega q^{n+1}\chi\, d\underset{\sim}{x}\ ,\quad \chi \varepsilon M_p,$$

for n=0, ..., N-1.

The boundary terms generated by integration by parts in the formulation of the above variational equations are all equal to zero due to the no-flow boundary conditions assumed in (6)-(7). If inhomogeneous flow conditions had been specified in (6)-(7), then the transformation to the non-divergence form utilized to define the modified method of characteristics would have introduced some nonlinear boundary terms which must be treated carefully and incorporated in (23). For details of how to treat these inhomogeneous boundary conditions, see Ref. 8.

From (23), one can easily see the importance of the Darcy velocity in the concentration equation. In the first place, the diffusion-dispersion tensor $\underset{\sim}{D}$ from (3) depends explicitly upon $\underset{\sim}{u}$, not upon the pressure p. Inaccurate velocities will thus affect both the directional dependence and the amount of dispersion in the problem.

Also, since the characteristic directions are determined directly from the Darcy velocities, our modified method of characteristics time-stepping procedure depends heavily upon accurate velocity approximation. If the computed velocities are inaccurate, so are the tangents to the characteristics at the grid points and the determination of the $\bar{\underset{\sim}{x}}$'s from (18). This can be the source of mass

balance errors in the calculation of the concentrations from (23).

Finally, the use of (24) to obtain Darcy velocities enhances problems caused by sharply changing permeabilities or viscosities. In finite difference methods or in finite element methods using (24), an approximate P is determined, subject to discretization errors; then this approximation is differenced or differentiated to obtain a less accurate (in general) and often rough approximation to $\underset{\sim}{u}$. Then this result is multiplied by a possibly rapidly changing coefficient k/μ to obtain a fairly rough approximation to $\underset{\sim}{u}$. The physical velocities are in general much smoother functions because rapid changes in k/μ are compensated for by corresponding rapid changes in ∇p. In this paper, we consider the use of mixed finite element methods to approximate the Darcy velocities in a more accurate fashion as in Ref. 9.

MIXED FINITE ELEMENT METHOD

In the mixed finite element method, we solve equation (1) for both the pressure and the velocity simultaneously via a system of first order partial differential equations. By solving for $-k/\mu\nabla p$ as one term, we minimize the difficulties caused by rough coefficients k/μ in standard methods. See Ref. 9 and 10 and the discussion of numerical results below for examples of how mixed methods treat widely varying coefficients in an accurate manner.

Let $L^2(\Omega)$ be the set of all functins on Ω whose square has finite integral. Let $H^1 = H^1(\Omega)$ consist of those functions in $L^2(\Omega)$ whose first-order partial derivatives are also in L^2. Let $H(\text{div}; \Omega)$ be the set of vector functions $\underset{\sim}{\chi}\varepsilon(L^2(\Omega))^2$ such that $\nabla \cdot \underset{\sim}{\chi}\varepsilon L^2(\Omega)$ and let

$$V = H(\text{div}; \Omega) \cap \{v \cdot \nu = 0 \text{ on } \partial\Omega\} . \tag{26}$$

Let $W = L^2(\Omega)$.

We recall from (1) the system of first-order partial differential equations for p and $\underset{\sim}{u}$ of the form,

$$\underset{\sim}{u} = -\frac{k}{\mu}\nabla p , \quad \underset{\sim}{x}\varepsilon\Omega, \ t\varepsilon J, \qquad \text{(Darcy's law)} \tag{27}$$

$$\nabla \cdot \underset{\sim}{u} = q , \quad \underset{\sim}{x}\varepsilon\Omega, \ t\varepsilon J. \quad \text{(conservation of mass)} \tag{28}$$

As in Ref. 9, we obtain the following weak form of (27)-(28) which determines our mixed method:

$$\iint_\Omega [\frac{\mu}{k}\underset{\sim}{u} \cdot \underset{\sim}{v} dx - \nabla \cdot \underset{\sim}{v} p] \, d\underset{\sim}{x} = 0 , \quad \underset{\sim}{v}\varepsilon V, \tag{29}$$

$$\iint_\Omega \nabla \cdot \underset{\sim}{u} \, w \, dx = \iint_\Omega q \, w \, dx , \quad w\varepsilon W. \tag{30}$$

Using the notation from (22), we next define the finite dimensional subspaces of V and W from which we will approximate $\underset{\sim}{u}$ and p. Letting Δ_x^p and Δ_y^p denote the x and y partitions for the pressure equation, we define

$$W_h = M_{-1}^1(\Delta_x^p) \otimes M_{-1}^1(\Delta_y^p) , \tag{31}$$

$$\tilde{V}_h = (M_0^2(\Delta_x^p) \otimes M_{-1}^1(\Delta_y^p)) \times (M_{-1}^1(\Delta_x^p) \otimes M_0^2(\Delta_y^p)) \tag{32}$$

$$V_h = \{\underset{\sim}{v}\varepsilon\tilde{V}_h : \underset{\sim}{v} \cdot \underset{\sim}{\nu} = 0 \text{ on } \partial\Omega\} . \tag{33}$$

(We note that a C^{-1} function is a discontinuous function.) These spaces are special cases of those defined by Raviart and Thomas[11]. Thus W_h contains discontinuous linear functions in x tensored with discontinuous linears in y. Also the x-component of V_h is composed of C^0 quadratics in x tensored with discontinuous linears in y and the y-component of V_h is composed of discontinuous linears in x tensored with C^0 quadratics in y. Note that $W_h \subset W$, $V_h \subset V$ and $V_h \subset V$.

In order to treat the point sources and sinks which model wells in our codes, we subtract out the logarithmic singularities at the wells and solve for the remaining portion of the velocities. As in Ref. 9, decomposing $\underset{\sim}{u}$ into its regular and singular parts ($\underset{\sim}{u}_r$ and $\underset{\sim}{u}_s$, respectively), we obtain

$$\underset{\sim}{u} = \underset{\sim}{u}_r + \underset{\sim}{u}_s , \tag{34}$$

$$\underset{\sim}{u}_s = \sum_{j=1}^{N_w} Q_j(t) \nabla N_j , \tag{35}$$

$$N_j = \frac{1}{2\pi} \log |x - x_j| , \quad j=1, \ldots, N_w, \tag{36}$$

where N_w is the number of wells, $Q_j(t)$ are the flow rates at the wells located at x_j, and $\underset{\sim}{u}_r$, the regular part of $\underset{\sim}{u}$, satisfies the relations

$$\nabla \cdot \underset{\sim}{u}_r = 0 , \quad \underset{\sim}{x}\varepsilon\Omega, \tag{37}$$

$$\underset{\sim}{u}_r \cdot \underset{\sim}{\nu} = -\underset{\sim}{u}_s \cdot \underset{\sim}{\nu} , \quad \underset{\sim}{x}\varepsilon\partial\Omega, \tag{38}$$

for $t\varepsilon J$. Let $\underset{\sim}{U}_r$ be the finite element approximation to $\underset{\sim}{u}_r$ from $\tilde{V}_h$, let

$$\underset{\sim}{U} = \underset{\sim}{U}_r + \underset{\sim}{u}_s \tag{39}$$

be our numerical approximation of $\underset{\sim}{u}$, and let $P\varepsilon W_h$ be our approximation to p. We then see that, for any n, $\underset{\sim}{U}_r^n$ satisfies the discrete mixed method equations:

$$\iint_\Omega [\frac{\mu(C^n)}{k}\underset{\sim}{U}_r^n \cdot \underset{\sim}{v} - \nabla \cdot \underset{\sim}{v} P^n] \, d\underset{\sim}{x} = -\iint_\Omega \frac{\mu(C^n)}{k}\underset{\sim}{u}_s \cdot \underset{\sim}{v} \, d\underset{\sim}{x} , \quad \underset{\sim}{v}\varepsilon V_h, \tag{40}$$

$$\iint_\Omega \nabla \cdot \underset{\sim}{U}_r^n \, w \, d\underset{\sim}{x} = 0 , \quad w\varepsilon W_h, \tag{41}$$

$$\iint_{\partial\Omega} (\underset{\sim}{U}_r^n + \underset{\sim}{u}_s) \cdot \underset{\sim}{\nu}(\underset{\sim}{v} \cdot \underset{\sim}{\nu}) \, ds = 0 , \quad \underset{\sim}{v}\varepsilon V_h. \tag{42}$$

We note that (42) requires that the net flow across $\partial\Omega$ of each boundary element be zero.

We can now define our fully discrete method utilizing mixed methods and the method of characteristics to be the system described by (5)-(7), (23), and (35)-(42). We note that the $\underset{\sim}{U}^*$ required for (23) now denotes the approximate average of the Darcy velocity approximations obtained from the

mixed method (40)-(42) and not the $\underline{u}^*$ obtained via (24). The new velocity approximations are more accurate and introduce less error into the concentration equation. The concentration equation is decoupled in time from the mixed method equations and can be solved very efficiently in a sequential time-stepping mode. First the concentration C^{n+1} is obtained at the advanced time-level using extrapolated velocities from previous time-levels. Then the mixed method is applied using that C^{n+1} to obtain p^{n+1} and $\underline{u}^{n+1}$ with no additional time-truncation error. Theoretical results for this method are described below.

We note that this sequential procedure could be iterated by using the computed $\underline{u}^{n+1}$ in place of the extrapolation continuing until convergence. The present scheme would be the first iteration. This was not attempted in this study; it may be of use in more complicated applications.

THEORETICAL RESULTS

The modified method of characteristics time-stepping procedure was analyzed in Ref. 7 for general linear convection-diffusion equations coupled with either a finite difference or a finite element spatial discretization. For the Galerkin case with piecewise-polynomials of degree r, and Δx mesh spacing, the error in the numerical solution is bounded by $K(\Delta x^{r+1} + \Delta t)$, where K is a constant which is independent of Δx and Δt. These are termed optimal-order spatial estimates. For central finite differences, convergence in space was shown to be second-order with uniform grid (provided that the interpolation to $\bar{x}$ in (18) was based on quadratic functions) and first-order with non-uniform grid. In the time discretization error estimates, since $\frac{\partial}{\partial t}$ was replaced by $\frac{\partial}{\partial \tau}$, the $\frac{\partial^2 c}{\partial t^2}$ terms in the truncation error estimates are replaced by $\frac{\partial^2 c}{\partial \tau^2}$, a term which is, in general, much smaller. See Ref. 12 for a more complete discussion of this advantage of modified method of characteristics procedures. Therefore, with a given spatial discretization, it is possible to take much larger time steps with characteristic methods than with standard procedures, without loss of accuracy.

Analyses for Galerkin methods for the miscible displacement problem described above assuming smoothly distributed sources and sinks and standard backward Euler time-stepping methods have appeared in other papers by the authors[13,8]. In these papers optimal order spatial error estimates were obtained for the concentration equation, but not for the velocity terms. Using mixed methods for approximating the velocities in the coupled systems allowed fully optimal order spatial convergence estimates for the same problem to be obtained by Douglas and two of the authors[14,15]. The characteristic time-stepping procedure was analyzed for the same problem by Russell in Ref. 16. Analysis for the combination of characteristic time-stepping and mixed methods will appear in a forthcoming paper by the authors.

The use of point sources and sinks in the model described in this paper degrades the smoothness of the unknowns p and $\underline{u}$ around the wells and hence the accuracy of the approximations in these regions. An analysis for the miscible displacement problem in the constant viscosity (unit mobility ratio) case using point sources and sinks was presented in Ref. 17.

VISCOUS FINGERING

A severe difficulty in the numerical modeling of enhanced recovery processes is the need to incorporate in our simulation models the bypassing of oil due to a viscous fingering phenomenon. The conservation equations presented in (1)-(2) were derived via a volume averaging mechanism which does not model physical behavior on a pore-volume scale. Since these mathematical equations are not capable of describing the physics of the instabilities on the microscopic level due to viscosity differences, they should not be expected to model fingering on that level. If, however, heterogeneous rock properties are described on a large enough scale that they can be incorporated in the permeabilities on a grid-size level, then the results of the mathematical model should reflect these heterogeneities in the form of a macroscopic fingering phenomenon due to varying flow velocities. Since our mathematical model includes differences in longitudinal versus transverse dispersion levels from (3), the fingers initiated by the variable permeabilities should propagate and grow in a manner akin to viscous fingering on a smaller scale. If our model did not include permeability variations or longitudinal dispersion effects, any fingering phenomenon noticed would be due to numerical errors and not to the modeling of any physics.

An example of fingering induced by a cell-sized permeability variation and enhanced by longitudinal dispersion effects is shown in Figure 6 and is described in more detail in the numerical results section below. At present, our mathematical model is not capable of incorporating viscous fingering effects which initiate on a microscopic, pore-volume level. Techniques such as those presented by Koval[18] will be required to model this behavior.

COMPUTATIONAL FEATURES AND NUMERICAL RESULTS

Near the injection well, in the early stages of displacement, the front is very sharp and travels quickly. A radial initialization to allow easy start up was utilized. This initialization procedure is discussed in Ref. 5.

The need to reach back along the characteristics longer distances near the wells due to larger velocities must be treated carefully. The segmenting description to treat this problem was presented above. Also special Labatto quadrature methods used around the wells were presented in Ref. 5.

Special techniques for treating the mixed finite element methods have been described by the authors[9,10]. In earlier work[9], a good preconditioner for the iterative solution of the system (40)-(42) had not been found. Recently Wheeler and Gonzales have shown that the finite difference matrix for the pressure equation (25) is a good preconditioner for the mixed finite element methods discussed here, and the overall method is computationally attractive. The sequential time-stepping procedure is similar to that presented in Ref. 5.

The time stepping procedure presented here does not conserve mass, and maintaining a good material balance is one of its most problematic aspects. A variational method based upon the non-divergence form (9) will have additional material balance errors due to interior errors in the velocity solution. This is one of the major motivations for obtaining more accurate velocity approximations via mixed methods. To emphasize the effects of using the method of characteristics, we substitute $\theta = 1$ in equation (23). Assuming that $C^{n+1} = \tilde{C}^{n+1}$ at injection wells, (23) yields

$$(43) \quad \int\int_{\Omega} \phi\, C^{n+1}\, d\underset{\sim}{x} = \int\int_{\Omega} \phi\, C^{n}(\tilde{\underset{\sim}{x}})\, d\underset{\sim}{x} ,$$

which says that the total mass of the injected components is solely dependent upon the mass at time level t^n and the characteristics that track the convection in time. Thus accurate velocities and quadratures are imperative for good material balance control.

In Table 1, we present results of several different simulations with adverse mobility ratios (M = 10, 41, 100). The numerical experiments simulated miscible displacement for one-quarter of a regular five-spot pattern with injection and production wells at the corners of the domain. The side of the quarter five-spot was 1000 feet, the permeability was set to 100 md., and the porosity was 0.1. Oil viscosity was 1 cp and the well rates were 200 cu. ft./D per foot of formation. One pore volume was injected in 2000 days; we henceforth refer to time in units of pore volumes (PV).

The concentration grids were nonuniform with finer subdivisions near the wells. For more details of specific grids, see Ref. 5. The pressure grids were uniform, but of different size than the concentration grids. These sizes are labeled in Table 1 for each run. We found that time steps in the range of .01 PV to .04 PV were appropriate with this method. These are larger by an order of magnitude than time steps required for comparable methods not utilizing the method of characteristics. This is an important feature of our methods.

The maximum overshoot (approximations with $C^n > 1$) and undershoot (approximations with $C^n < 0$) were controlled, being everywhere less than 3.5% even on coarse (20 x 20) concentration grids. The overshoot and undershoot occurred only in the neighborhood of the moving front and did not persist as the front moved on. Thus they are not instabilities in the method, but merely indications that the grids chosen were too coarse to accurately resolve the very sharp fronts caused by high mobility ratios and dispersion ratios. As the grid was refined, the overshoot and undershoot were reduced correspondingly. Maximum overshoot errors occurred near the production well where extremely sharp fingering into the well was simulated. Table 1 shows that, in spite of overshoot and undershoot problems and mass balance problems mentioned above, the material balance errors were uniformly below 0.5%, except for the one case with M = 41 where the error was 1.7%.

Recovery curves and concentration profiles, shown in Figures 2, 3, and 4 show that these methods exhibit very little grid-orientation problems. The 20 x 20 concentration grids had diagonal grid orientation (see Ref. 19) while the 28 x 28 concentration grids had a parallel grid orientation. Recoveries at 1 PV injected for various problems and orientations are presented in Table 1.

In order to emphasize the need for accurate velocities in difficult problems using the method of characteristics, we present two concentration maps for the same problem and different grid sizes when C^0 quadratics were used for pressure approximations in the system (23)-(25). Using a 32 x 32 concentration grid, unstable fingers were predicted; Figure 5a shows concentration level curves for this case. When the grid was refined to a 64 x 64 level, the fingers diappeared; Figure 5b shows concentration level curves for this case. Using mixed finite element methods for the 32 x 32 case, results were obtained which were essentially identical to Figure 5b, eliminating the spurious fingering prediction obtained using standard finite element methods with C^0 quadratics for pressure. Since the permeabilities were assumed to be constant in these runs, and no fingering phenomenon was included in the numerical model, the fingers should not appear.

In order to illustrate that our model will propagate fingers due to grid-sized permeability variations, we simulated a problem with M = 100, $\phi d_m = 0$, $\phi d_\ell = 10$, and $\phi d_t = 1$ where a random number generator was used to set random, grid-sized permeability variations. The randomly chosen permeabilities varied between 0.002 and 1016. The results of the fingering produced by these varying permeabilities is presented in Figure 6.

CONCLUSIONS

The combination of finite elements for concentration, mixed finite elements for pressure and velocities, and methods-of-characteristic time-stepping methods can simulate miscible displacements with adverse mobility ratios accurately with time steps an order of magnitude larger than those used in standard methods.

These simulations predict recovery accurately and exhibit minimal grid orientation, numerical dispersion, and overshoot. The overshoot and undershoot reflect the inability to resolve very sharp fronts on coarse meshes and not stability problems.

These techniques can treat large mobility ratios (M = 10, 41, 100), widely varying permeabilities, fairly coarse grids, and anisotropic dispersion in tensor form.

These methods do not model microscopic viscous fingering phenomena but will propagate fingers generated by grid-sized permeability variations.

Care must be taken to treat characteristics around the wells, across flowing boundaries, and in general in order that material balance errors can be controlled.

NOMENCLATURE

a_x, a_y - endpoints of the spatial domain, ft.

b_x, b_y - endpoints of the spatial domain, ft.

c - concentration of the invading fluid, dimensionless

c_0 - initial concentration, dimensionless

$\tilde{c}$ - source or sink concentrations, dimensionless

C^n - approximation to concentration, dimensionless

d_m - molecular diffusivity, sq. ft./D

d_ℓ - longitudinal dispersivity, ft.

d_t - transverse dispersivity, ft.

$\underset{\approx}{D}$ - dispersion tensor, sq. ft./D

$\underset{\sim}{Eu}$ - linearly extrapolated velocity, ft./D

J - time interval, days

k - permeability of the reservoir, md

M_j^n - piecewise polynomial function spaces

M - mobility ratio

N - number of time steps to the final time

N_x, N_y - number of elements in the x or y direction

p - pressure of the total fluid, psi

P^n - approximation to pressure, psi

P_m - polynomials of degree m or less

q - volumetric flow rate at the wells, sq. ft./D

t, t^n - time or time level, days

T - final time, days

$\underset{\sim}{u}$ - total fluid velocity, ft./D

$\underset{\sim}{u}_r$, $\underset{\sim}{u}_s$ - regular and singular parts of $\underset{\sim}{u}$, ft./D

$\underset{\sim}{U}^n$, $\underset{\sim}{U}_r^n$ - approximations to $\underset{\sim}{u}$ and $\underset{\sim}{u}_r$, ft./D

v, w - one-dimensional linear basis functions

V, $\tilde{V}$ - function spaces for velocities

V_h, $\tilde{V}_h$ - mixed finite element spaces for velocities

W, W_h - function spaces for pressures

$\underset{\sim}{x}$ - Cartesian coordinate vector (x, y), ft.

$\bar{\underset{\sim}{x}}$ - point reached by moving back along a characteristic from $\underset{\sim}{x}$

Δt, Δt_n - time step and intermediate time step, days

Δx - spatial discretization level, ft.

Δ_x^c, Δ_y^c - spatial grids for concentration, ft.

Δ_x^p, Δ_y^p - spatial grids for pressure, ft.

θ - test functions for concentration

μ - viscosity of the fluid, cp

$\underset{\sim}{\nu}$ - outward unit normal vector (ν_1, ν_2) to $\partial\Omega$

χ - test functions for pressures

ϕ - porosity of the reservoir, dimensionless

τ - unit vector in the characteristic direction

Ω - spatial domain, sq. ft.

$\partial\Omega$ - boundary of Ω

ACKNOWLEDGMENTS

The authors wish to thank Mobil Research and Development Corporation and Marathon Oil for permission to publish this paper.

REFERENCES

1. Settari, A., Price, H.S., and Dupont, T., "Development and Application of Variational Methods for Simulation of Miscible Displacement in Porous Media," Soc. Pet. Eng. J. (June 1977), pp. 228-246; Trans., AIME, Vol. 263.

2. Young, L. C., "A Finite-Element Method for Reservoir Simulation," Soc. Pet. Eng. J. (Feb. 1981), pp. 115-128.

3. Peaceman, D. W., Fundamentals of Numerical Reservoir Simulation, Elsevier North-Holland, New York, 1977.

4. Peaceman, D. W., "Improved Treatment of Dispersion in Numerical Calculation of Multidimensional Miscible Displacement," Soc. Pet. Eng. J. (Sept. 1966), pp. 213-216.

5. Russell, T. F., "Finite Elements with Characteristics for Two-Component Incompressible Miscible Displacement," SPE 10500, Proc. Sixth SPE Symp. on Reservoir Simulation, New Orleans, LA, Jan. 1-Feb. 3, 1982.

6. Cavendish, J. C., Price, H. S., and Varga, R. S., "Galerkin Methods for the Numerical Solution of Boundary Value Problems," Soc. Pet. Eng. J. (June 1969), pp. 204-220; Trans., AIME, Vol. 246.

7. Douglas, J., Jr., and Russell, T. F., "Numerical Methods for Convection-Dominated Diffusion Problems Based on Combining the Method of Characteristics with Finite Element or Finite Difference Procedures," SIAM J. Numer. Anal. (to appear).

8. Ewing, R. E., and Russell, T. F., "Efficient Time-stepping Procedures for Miscible Displacement Problems in Porous Media," SIAM J. Numer. Anal. 19 (1982), pp. 1-67.

9. Darlow, B. L., Ewing, R. E., and Wheeler, M. F., "Mixed Finite Element Methods for Miscible Displacement Problems in Porous Media," SPE 10501, Proc. Sixth SPE Symp. on Reservoir Simulation, New Orleans, LA, Jan. 31-Feb. 3, 1982, pp. 137-145; Soc. Pet. Eng. J. (to appear).

10. Ewing, R. E., and Wheeler, M. F., "Computational Aspects of Mixed Finite Element Methods," Numerical Methods for Scientific Computing, R. S. Stepleman, ed., North Holland Publ. Co. (to appear).

11. Raviart, P. A., and Thomas, J. M., "A Mixed Finite Element Method for 2-nd Order Elliptic Problems," Mathematical Aspects of the Finite Element Method, Rome 1975, Lecture Notes in Mathematics, Springer-Verlag, Heidelberg (1977).

12. Ewing, R. E., and Russell, T. F., "Multistep Galerkin Methods along Characteristics for Convection-Diffusion Problems," Advances in Computer Methods for Partial Differential Equations - IV, R. Vichnevetsky and R. S. Stepleman, eds., IMACS, Rutgers Univ., New Brunswick, NJ, 1981, pp. 28-36.

13. Ewing, R. E., and Wheeler, M. F., "Galerkin Methods for Miscible Displacement Problems in Porous Media," SIAM J. Numer. Anal. 17 (1980), pp. 351-365.

14. Douglas, J., Jr., Ewing, R. E., and Wheeler, M. F., "The Approximation of the Pressure by a Mixed Method in the Simulation of Miscible Displacement," R.A.I.R.O. Analyse Numérique (to appear).

15. Douglas, J., Jr., Ewing, R. E., and Wheeler, M. F., "Time-stepping Methods for Simulation of Miscible Displacement Using Mixed Methods for Pressure Approximation," R.A.I.R.O. Analyse Numérique (to appear).

16. Russell, T. F., "An Incompletely Iterated Characteristic Finite Element Method for a Miscible Displacement Problem," Ph.D. Thesis, Univ. of Chicago, 1980.

17. Ewing, R. E., and Wheeler, M. F., "Galerkin Methods for Miscible Displacement Problems with Point Sources and Sinks - Unit Mobility Ratio Case," Proc. Spec. Year in Numer. Anal., Univ. of Maryland, College Park, MD, Lecture Notes #20, 1981, pp. 151-174.

18. Koval, E. J., "A Method for Predicting the Performance of Unstable Miscible Displacement Instability," Soc. Pet. Eng. J. (June 1963), pp. 145-154.

19. Yanosik, J. L., and McCracken, T. A., "A Nine-point Finite-difference Reservoir Simulator for Realistic Prediction of Unfavorable Mobility Ratio Displacement," Soc. Pet. Eng. J. (Aug. 1979), pp. 253-262; Trans., Aime, Vol. 267.

Table 1

Numerical Results for Adverse Mobility Ratios

M	ϕd_m	ϕd_ℓ	ϕd_t	C-grid	P-grid	ΔT (PV)	Recovery (PV-1 PV injected)	Material in Place (PV)	Maximum Overshoot or Undershoot
10	1	0	0	20x20	10x10	.02	.7347	1.0015	.019
10	0	10	1	20x20	15x15	.02	.6649	.9939	.023
10	0	10	1	28x28	20x20	.02	.6559	1.0051	.028
41	0	10	1	32x32	20x20	.02	.5470	.9833	.019
100	1	0	0	20x20	15x15	.02	.6983	.9946	.035
100	1	0	0	28x28	20x20	.02	.6700	.9967	.035

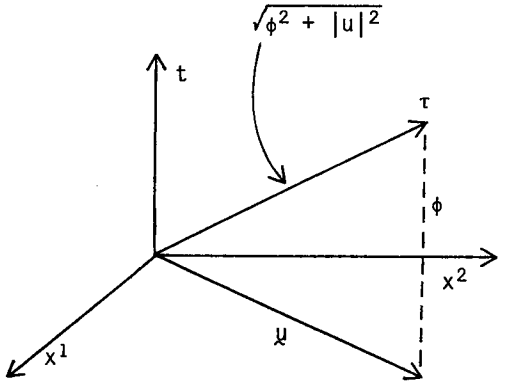

Figure 1: Characteristic Direction

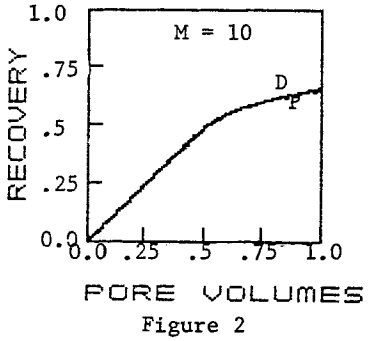

Figure 2
Recovery Curves
ϕd_m=0, ϕd_ℓ=10, ϕd_t=1

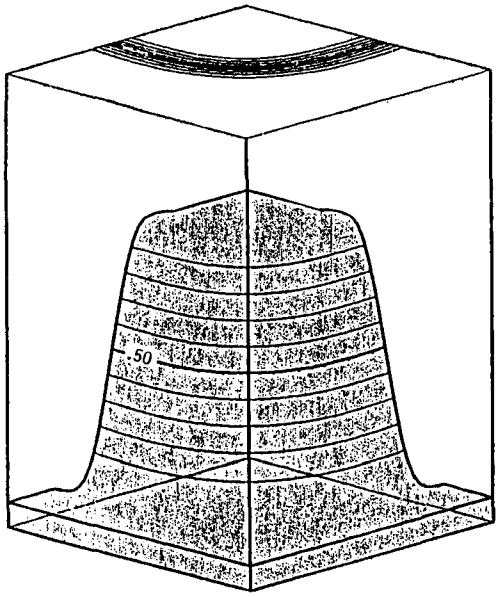

Diagonal Orientation
20x20 Concentration 15x15 Pressure

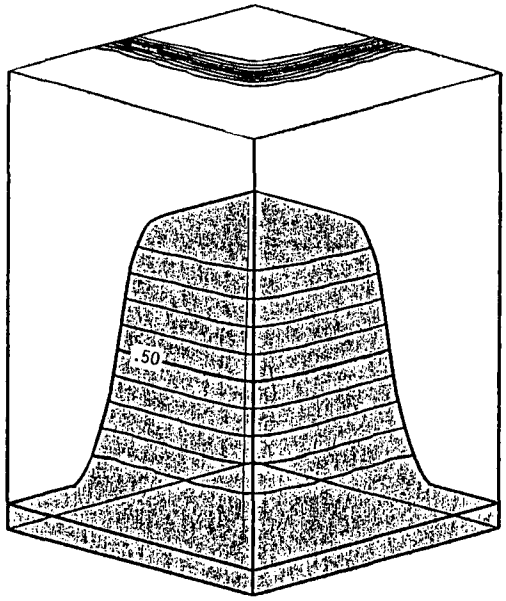

Parallel Orientation
28x28 Concentration 20x20 Injected

$M = 10,\ \phi d_m = 0,\ \phi d_\ell = 10,\ \phi d_t = 1$

Figure 3: Concentration Profile - .3 PV Injected

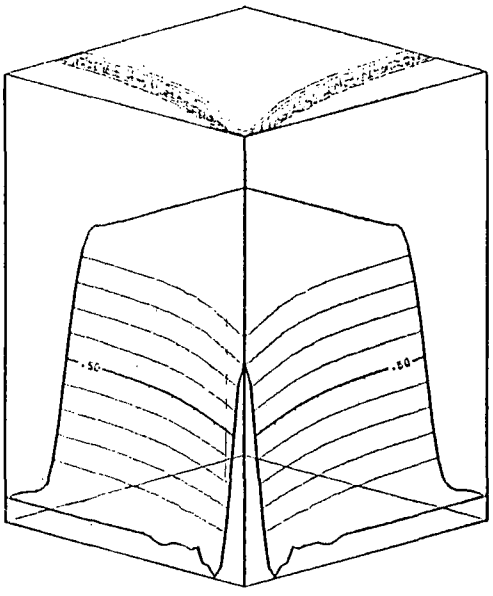

Diagonal Orientation
20x20 Concentration 15x15 Pressure

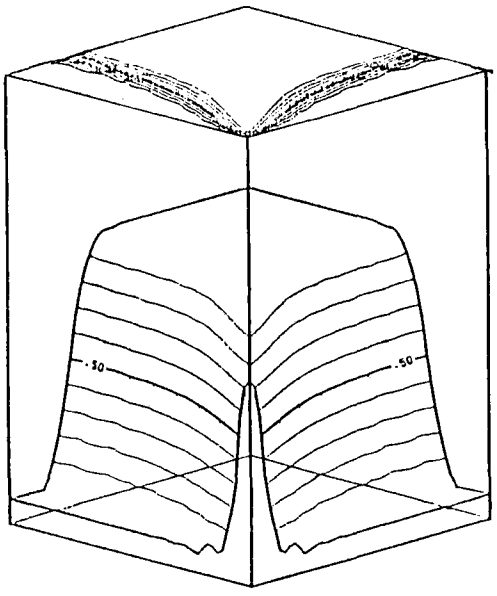

Parallel Orientation
28x28 Concentration 20x20 Injected

$M = 10,\ \phi d_m = 0,\ \phi d_\ell = 10,\ \phi d_t = 1$

Figure 4: Concentration Profile - 1 PV Injected

a

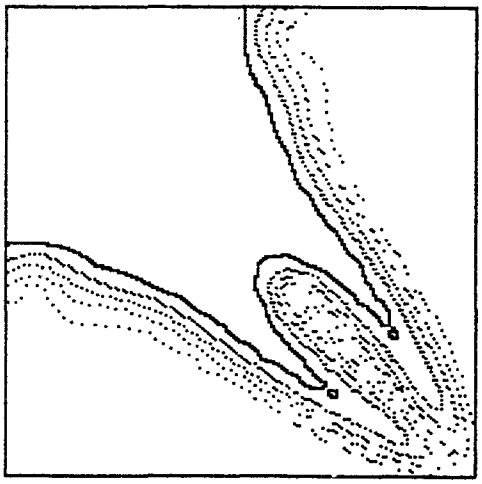

32x32 Concentration
20x20 C^0 Quadratic Pressure
.5 PV Injected

b

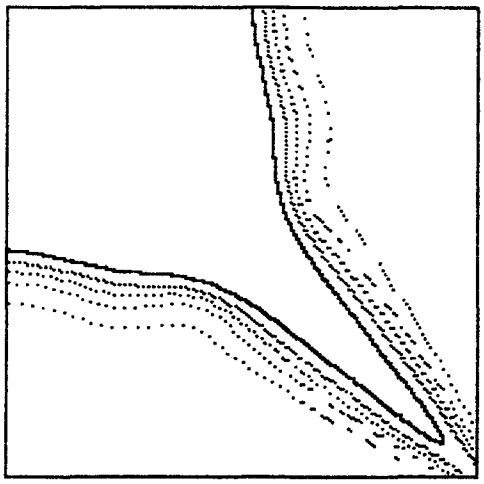

64x64 Concentration
32x32 C^0 Quadratic Pressure
.5 PV Injected

Figure 5: Numerical Fingering

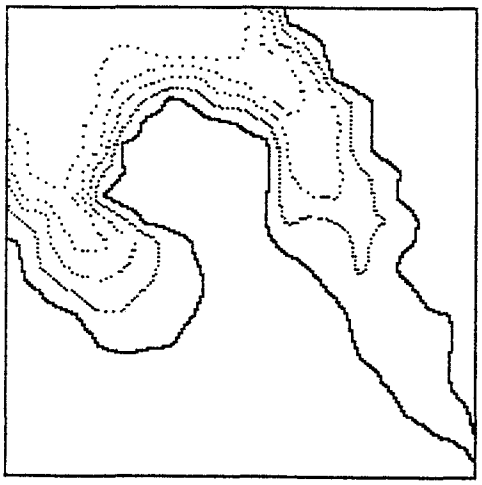

Figure 6: Fingering for Variable Permeability